Nonlinear Hall effect for a two-dimensional electron gas in a cylindrical nanomembrane

Julia S. Vorobyova,* Alexander B. Vorob'ev, Victor Y. Prinz, and Alexander I. Toropov
Rzhanov Institute of Semiconductor Physics, Siberian Branch of Russian Academy of Science, pr. Lavrentieva 13, 630090 Novosibirsk, Russia

(Received 17 April 2018; revised manuscript received 22 July 2018; published 1 October 2018)

A detailed study of the effect due to Lorentz-force gradient on the Hall voltage of a two-dimensional electron gas (2DEG) was carried out on specially prepared cylindrical nanomembranes with 2DEG. In the fabricated nanomembranes, weak and strong magnetic-field gradients and, also, sign-alternating magnetic fields acting on the electrons in the nanomembranes were obtained. It was found that an increase in the magnetic-field gradient led to an increase of the Hall constant of 2DEG in weak fields, whereas a change in the field sign caused an inversion of this constant in weak fields. An explanation based on the analysis of the dependence of electron drift velocities on the magnetic field gradient is proposed. The investigated system is of interest both for applications and fundamental research.

DOI: 10.1103/PhysRevB.98.165401

I. INTRODUCTION

Spatially nonuniform magnetic fields play an important role in various physical and technological areas as they offer additional possibilities for controlling both the spin and dynamics of charged particles. Such fields were used in the famous Stern-Gerlach experiment; magnetic-field gradients are presently used in magnetic resonance imaging; and in nuclear physics such gradients are used for plasma confinement. Fabrication of spin filters based on semiconductor heterostructures with two-dimensional electron gas (2DEG) [1] and graphene sheets [2] placed in a nonuniform magnetic field was proposed. A magnetic-field gradient leads to a Lorentz-force gradient and to a gradient of the Larmor radii. As a result, circular orbits observed in uniform magnetic fields transform into cycloid orbits. The drift velocity of electrons captured to those trajectories is normal both to the magnetic field and to the magnetic-field gradient. If an electron passes regions having opposite magnetic-field vector directions, snakelike trajectories are formed [3]. For generation of a nonuniform magnetic field in a planar 2DEG, the local sputtering of magnetic materials [4–9] or the growth of heterostructures with a 2DEG on a faceted surface [10–12] was used. The latter approaches were used to obtain a stepwise profile of magnetic field with 1-T characteristic field changes over distances of 200 nm. Fabrication of structures with a smooth and controllable magnetic-field gradient by the above methods seems not to be possible; accordingly, the electron transport under smooth spatial variation of magnetic field remains almost fully unstudied. It should also be noted that magnetic field gradient and concentration gradient produce similar effects since the Hall resistance $R_{xy} = B/ne$, where B is the magnetic field and n is the density of charge carriers. A steplike electron density distribution was achieved in partially gated, doubly connected 2D GaAs/AlGaAs heterostructures [13,14]. A linear electron density distribution was obtained using the lateral photoeffect [15]. One more relevant study analyzes the effect of electron density distribution on the measurement of longitudinal resistance in quantum Hall systems [16].

The electrons in 2DEG experience the action due to the Lorentz force, defined by the surface-normal magnetic-field component B_n. In a 2DEG on a cylindrical surface placed in a magnetic field normal to the axis of the cylinder, the normal field component varies over the sample area according to the formula

$$B_n = B_0 \cos\varphi,$$

where B_0 is the applied magnetic field and φ is the angle between the normal to the surface and the vector B_0.

The gradient of B_n also varies along the cylinder surface of radius R:

$$\left|\text{grad}\, B_n\right| = \left|\frac{1}{R}\frac{\partial B_n}{\partial \varphi}\right| = \left|\frac{B_0}{R}\sin\varphi\right|.$$

In the present work we fabricated nanoshells with 2DEG shaped as cylinder sectors with current direction parallel to the cylinder axis. The angle α between the sector edges, and the angle φ of rotation of the sector around the cylinder's axis, both determine the spatial distribution of B_n and grad B_n. By varying these parameters, very interesting situations can be organized. For example, in a semicylinder ($\alpha = 180^\circ$) oriented with respect to the vector B_0 like it is shown in Fig. 1(a), the field B_n is modulated in amplitude, and it varies on the sample surface from 0 to B_0; the gradient of B_n changes its sign, and the absolute value of the gradient varies as well. If the semicylinder is oriented like in Fig. 1(b), then the field B_n varies not only in absolute value, it also change its sign, and the electron moves in a magnetic field that ranges from $-B_0$ to B_0. It is important that the field change preserves its sign in any external magnetic field. Contrary to this, in flat 2DEG with sputtered ferromagnets, such a situation is only possible in a very narrow interval of weak magnetic fields. For getting an idea about the ranges of involved variables, we can assess that for a 10° cylindrical sector with 10-μm radius placed in a

*Corresponding author: vorobyova@isp.nsc.ru

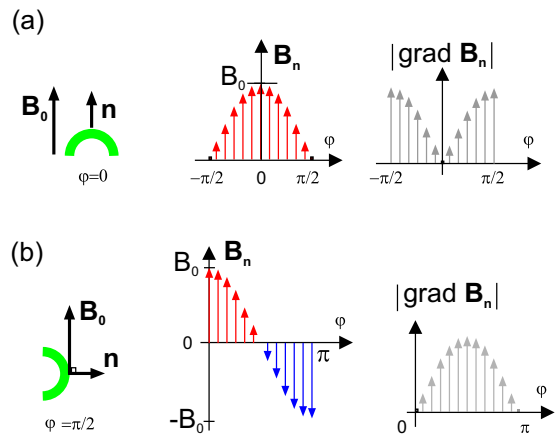

FIG. 1. Schematic distribution of the surface-normal magnetic-field component and its gradient for two orientations of a membrane shaped as a semicylinder with 2DEG.

magnetic field of 10 T, the drop of the field B_n on the surface of the sector can reach 1.7 T, and the gradient of B_n can exceed 10^6 T/m.

To summarize, the transport of a 2DEG on a cylindrical surface in a uniform magnetic field can be considered as the transport of a planar 2DEG in a strongly nonuniform, smoothly varying magnetic field. Various ranges of spatial variation of the surface-normal magnetic-field component, including sign-alternating ones, as well as those of its gradient, can be created. In turn, the geometric parameters of cylindrical shells allow one to preset and precisely control the type and distribution of electron trajectories. The sizes of the region with continuous variation of magnetic-field strength have allowed us to realize a situation with coexistent trajectories of all the three types: skipping, cycloid, and snakelike trajectories; this matter was theoretically analyzed by Müller [3].

The samples with 2DEG on a cylindrical surface were fabricated using the directional rolling procedure of strained heterofilms [17] with lithographically defined Hall bars. Earlier we have shown that in the cylindrical membranes with Hall bars in which the electric current flowed parallel to magnetic-field gradient [18], and in the helices [19], the redistribution of current density led to the vanishing of the longitudinal resistance and to a giant asymmetry of magnetoresistance at magnetic-field sign inversion ($R_{xx}(B)/R_{xx}(-B)$ reaches 10^4). The latter effect offers much promise for precise three-axis measurements of the direction and strength of magnetic fields. In quantizing fields, the effect is preserved, and it is attributed to the shortening of the oppositely directed edge states by magnetic-induced one-dimensional (1D) channels. The contribution due to such states into the net conductivity of samples was recently investigated by Nogaret *et al.* [20].

In the present study we experimentally examined the magnetotransport of 2DEG in semiconductor cylindrical nanomembranes. The Hall bars were oriented along the membrane, and the current was therefore directed normally to the magnetic-field gradient [Fig. 2(a)]. In the experiment, the distribution of the field B_n over the sample width and the drop of this field across the sample were variable quantities defined by the following parameters: (i) Hall-bar width (the smaller the Hall-bar width, the smaller the drop of the field B_n across the bar); (ii) angle of turn of the bar with respect

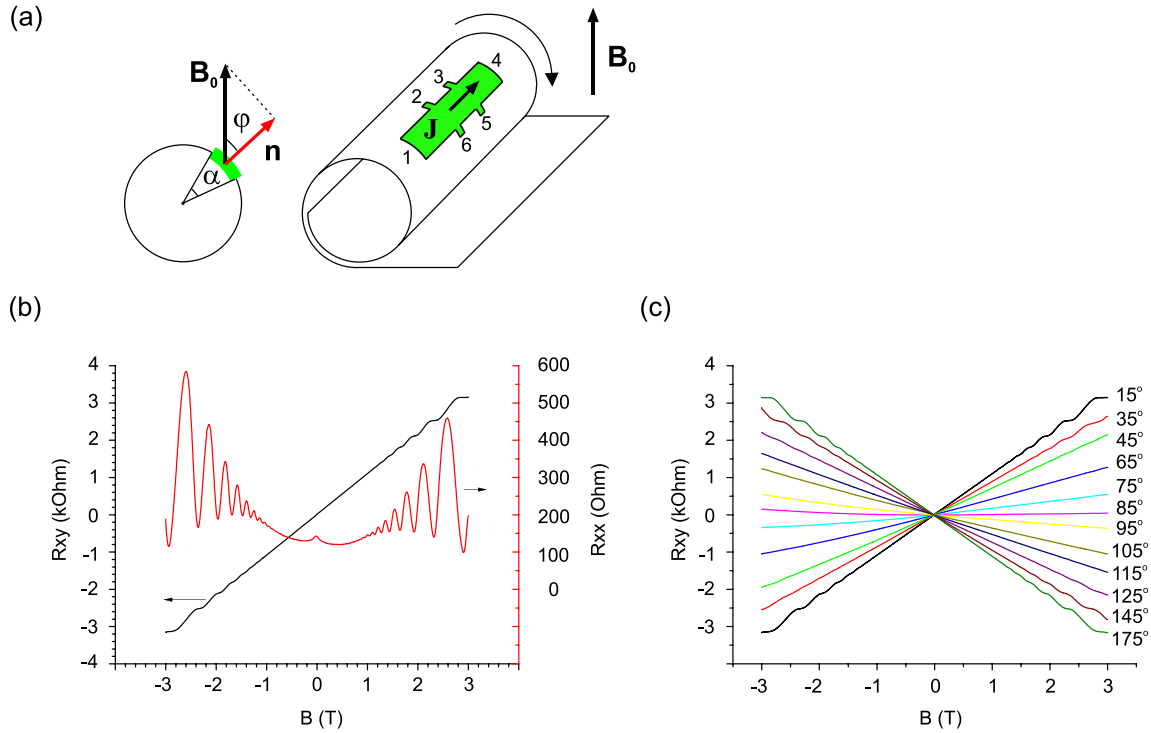

FIG. 2. (a) Experimental geometry, (b) dependence of the longitudinal and Hall resistances of the 2DEG on the magnetic-field strength in a 6-μm wide Hall bar, and (c) dependencies of Hall resistance on the magnetic field at various angles of rotation of the sample with respect to the direction of the external magnetic field.

to the direction of the external magnetic field B_0 (the larger the angle between the normal to the center of the bar and the external field, the larger the drop of B_n). The magnitude of the gradient of B_n and the possibility of its controllable variation right in the course of experiments have allowed us to reveal a nonlinear and nonmonotonic behavior of the Hall resistance as a function of external magnetic field for 2DEG moving along a cylindrical membrane.

II. EXPERIMENTAL RESULTS

The multilayered heterostructure was grown on a GaAs (100) substrate by molecular beam epitaxy (MBE) implemented on the Compact 21T system. After oxide removal, a smoothing GaAs layer was deposited onto the substrate to subsequently grow on this layer an AlAs/GaAs short-period superlattice (SPSL) providing for: (i) further smoothening of the growth surface, (ii) creation of a high-resistivity buffer layer intended for isolation of subsequent layers from the substrate, and (iii) trapping of impurities undergoing segregation from the substrate. The complete structure comprised a 50-nm-thick AlAs sacrificial layer and a 192-nm-thick strained multilayered film to be detached from the substrate. The multilayered film contained a 20-nm-thick $In_{0.18}Ga_{0.82}As$ stressor and the hereterostructure stack, including a 13-nm-thick central GaAs QW clad with δ-doped AlAs/GaAs SPSL spacers (a more detailed description of the epitaxial structure is given in Ref. [18]). The presence of two delta-doped layers on both sides of the quantum well makes it possible to obtain a structure with a symmetric potential promoting the attainment of a maximum concentration of charge carriers in the quantum well. Then, an $Al_{0.3}Ga_{0.7}As$ layer with a third embedded Si delta layer intended for compensation of the space-charge region inevitably arising on the surface of the structure was grown. Finally, a 5-nm-thick GaAs layer intended for protection of the AlAs-containing layers against oxidation and facilitating the preparation of ohmic contacts to the structure was grown.

The rolled-up Hall bars used in the present study were prepared by directional rolling of two-level lithography-defined mesastructures. The procedure for forming the scrolls with contacts was the one described in Refs. [18,19] except for the orientation of the Hall bar: in the present study the Hall bar was oriented along the axis of the cylinder. The scroll radius was 24 μm.

For obtaining different distribution of magnetic field in the 2DEG on a cylindrical surface, Hall bars of various widths (6, 16, and 75 μm) were prepared. The widest Hall bar had a largest angle between the lateral faces and, hence, the largest range of the surface-normal magnetic-field component over the surface. For instance, the 75-μm wide Hall bar occupied half the 24-μm radius circumference; hence, the magnetic field range in this Hall bar was the widest one. Intuitively, it was quite clear that the 2DEG in the narrow Hall bar would behave as a planar 2DEG, and the magnetic-field nonuniformity was expected to be manifested most brightly in the 2DEG transport in wide Hall bars. The rotation of the sample was performed during the measurements in liquid helium. A home-made rotating sample holder was used. The sample was oriented so that, during measurements, it was rotated around the cylinder axis. The experimental geometry is schematically depicted in Fig. 2(a). The external magnetic field was varied over the interval from -3 to 3 T.

The magnetic-field dependencies of the longitudinal and Hall resistances of 2DEG measured in the bent Hall bar of width 6 μm at $\varphi = 0$ are shown in Fig. 2(b). The Hall effect is linear with respect to magnetic field; in quantizing magnetic fields, a filling factor of $\nu = 8$ is achieved; and the positions of quantum Hall effect steps coincide with the minima of Shubnikov–de-Haas oscillations. The Fourier spectrum of Shubnikov–de-Haas oscillations versus the reciprocal magnetic field contains a single peak corresponding to a 2DEG concentration equal to $5.6 \times 10^{11}\,\mathrm{cm}^{-2}$. The Hall effect yields the same concentration, thus pointing to the absence of parallel conductions in our structure. The 2DEG mobility is $8 \times 10^4\,\mathrm{cm}^2/\mathrm{V\,s}$.

Consider first how the Hall dependencies evolve with the rotation of the cylindrical nanomembrane around its axis [Fig. 2(c)]. Evidently, here the Hall dependencies remain linear. In the course of the experiment, we additionally measured the turn angle with a standard Hall sensor and have found that the turn angles measured with the sensor and the turn angles calculated from the slope of the Hall dependence of the membrane were coincident. The peaks in the Fourier spectra of the dependencies $R_{xx}(B)$ also shifted with the turn through the angle corresponding to the Hall-sensor turn. All the observations indicated that, due to the small angular spacing α between the Hall contacts, 14°, the sample behaved like a planar sample with 2DEG placed in a tilted magnetic field.

Consider now what occurs in wider samples, with the drop of B_n across the sample being greater. Figure 3(a) schematically shows the experimental geometry in the case of a 16-μm-wide Hall bar. Here the angular spacing between the Hall contacts is 38°. The gradient of the surface-normal magnetic field component on the sample was controllably preset during the measurement process by turning the cylindrical nanomembrane around its axis. In the position with a maximum field B_0, the change of the surface-normal field is $0.06B_0$, whereas on the rotation into the region of $B_n = 0$ the difference between the values of B_n increases to $0.61B_0$. Under such conditions, the Hall dependencies exhibit a number of interesting features [Fig. 3(b)]. It is seen that the Hall effect at a near-zero angle φ is linear. On increasing the angle φ and, hence, on increasing the gradient of the field B_n, in the vicinity of zero there appears a curve portion with a larger slope than that in the strong fields. This effect is most pronounced when the edge of the sample reaches the line of $B_n = 0$ (Fig. 3, curve 6). At larger angles, when the field component on the sample changes its sign, the slope of the Hall dependence also changes its sign (Fig. 3, curve 7).

For gaining a deeper insight into the variation of the Hall effect in the presence of a magnetic-field gradient, we performed measurements on the Hall bar of width 75 μm, which value equaled half the circumference. The distribution of the normal magnetic-field component over the sample is shown in Fig. 4(b). Initially, the Hall dependencies show a slope reduced in weak fields (Fig. 4(c, d), curves 1 and 2), the slope changing its sign already at a small deviation from $\varphi = 0$ (Fig. 4(c, d), curves 3–7).

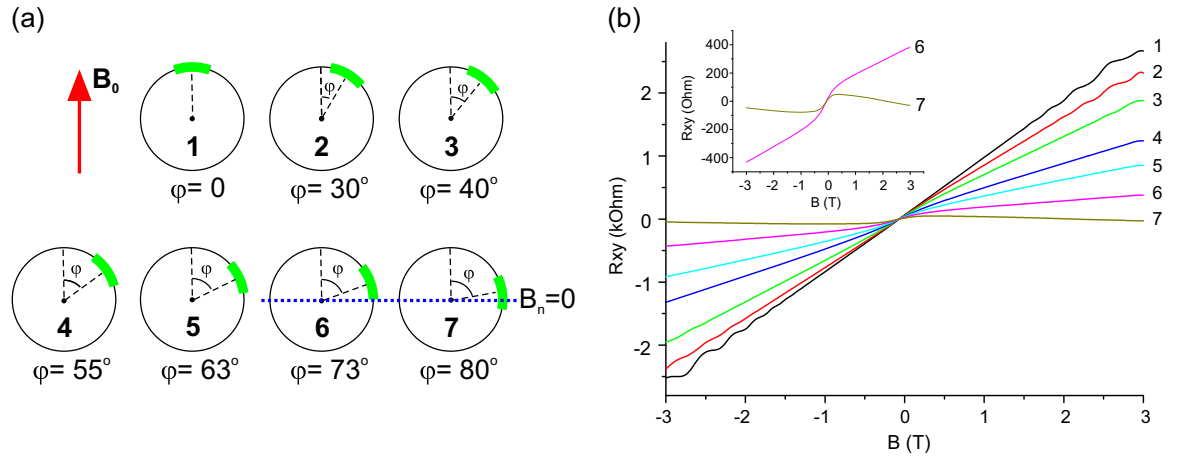

FIG. 3. (a) Schematic representation of the experimental geometry. Indicated are the angles of turn of the bent Hall bar with respect to the direction of the applied magnetic field, (b) dependence of the Hall resistance of 2DEG on the magnetic field in a Hall bar of width 16 μm at various turn angles of the sample. Curves 6 and 7 refer to the orientation with the maximum drop of the field B_n across the Hall bar. In the orientation corresponding to curve 7, the field B_n in the Hall bar changes its sign.

Thus, the brightest effect manifested by the Hall effect in 2DEG on a cylindrical surface is its nonlinearity. The nonlinearity is not observed in narrow Hall bars, and it becomes more pronounced on increasing the Hall-bar width, or the angle α between the lateral faces. Under certain conditions, the curve $R_{xy}(B)$ exhibits a curve portion with an opposite slope.

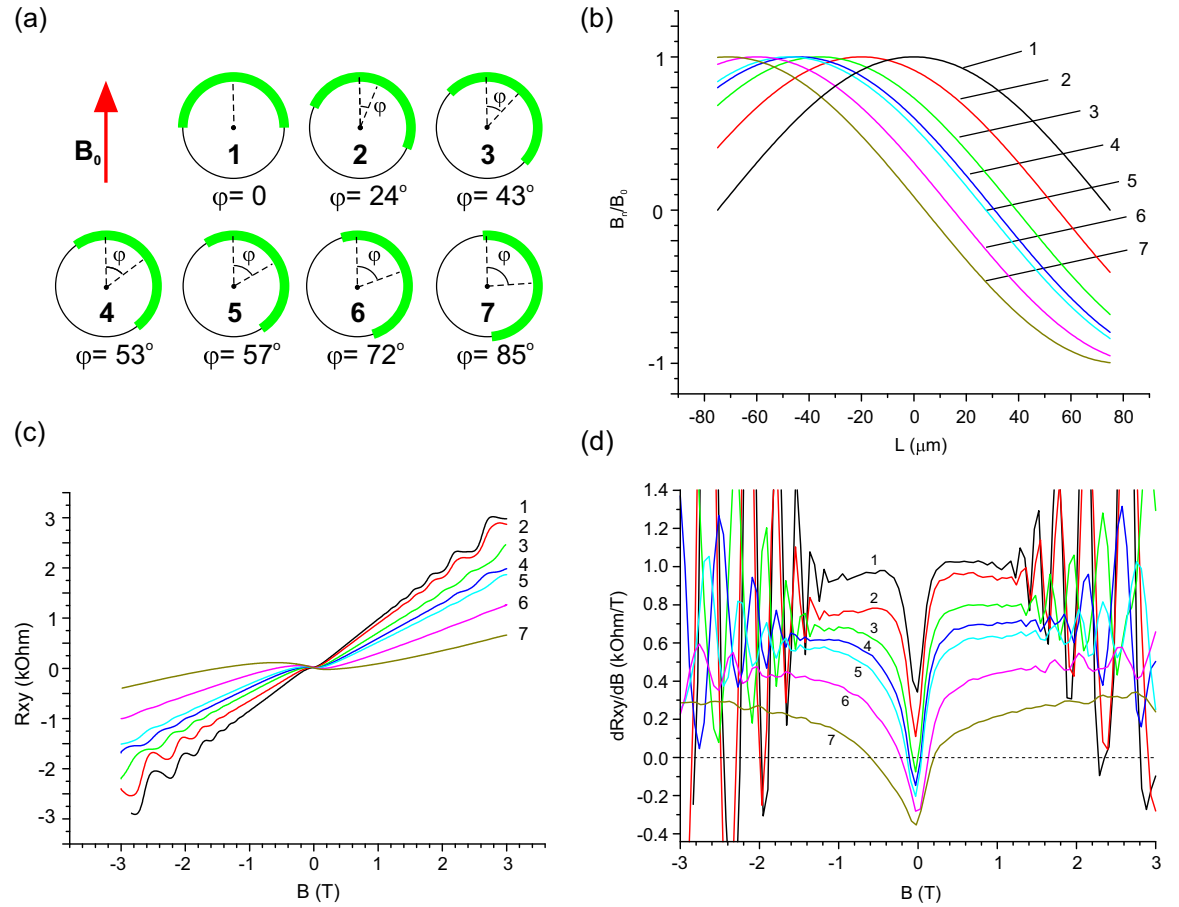

FIG. 4. (a) Schematic representation of the experimental geometry. Indicated are the angles of turn of the bent Hall bar of 75-μm width with respect to the direction of the applied magnetic field for the curves shown below, (b) the distribution of normal magnetic-field component over the width of the sample, (c) dependence of the Hall resistance of 2DEG on the magnetic field in the Hall bar at various turn angles of the sample, and (d) dependencies $dR_{xy}/dB(B)$ at various turn angles of the sample.

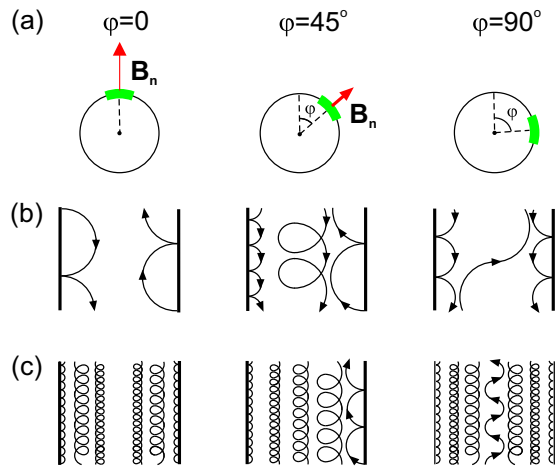

FIG. 5. (a) Experimental geometry for three different orientations of the membrane, (b) electron trajectories in the cylindrical nanomembrane in weak magnetic fields; Larmor radius r_c is close to the sample width W, $r_c \leqslant W$, and (c) electron trajectories in the cylindrical nanomembrane at $r_c \ll W$.

III. DISCUSSION

Below we give an explanation to the observed effects with reference to Fig. 5 in classical terms of electron orbits. Skipping orbits are formed along the sample boundary. Far from the edge, the cyclotron radius r_c changes continuously due to the gradient of B_n on the cylindrical surface, and cycloid trajectories are formed. The drift velocity of electrons captured by such trajectories is perpendicular both to the field B_n and to grad B_n. This is a gradient drift phenomenon considered in plasma physics [21]. If an electron crosses a line where $B_n = 0$, snakelike trajectories are formed. Only cycloid and skipping trajectories contribute to the Hall voltage. The snakelike trajectories on the cylindrical surface are symmetric about the zero-field line, $B_n = 0$; that is why the contribution into the Hall voltage due to the half-period with $B_n > 0$ in these trajectories is compensated with the contribution due to the half-period with $B_n < 0$. Let us consider the electron motion along cycloid trajectories in more detail.

The drift velocity of the electrons depends on the field B_n and on the gradient of this field [21]:

$$|v_H| = \frac{1}{2} r_c \,|\mathrm{grad}(r_c)\,|\omega_c = \frac{1}{2}\frac{e r_c^2}{m}\,|\mathrm{grad}(B_n)\,| = \frac{E_F}{e}\frac{|\mathrm{grad}(B_n)\,|}{B_n^2},$$

where r_c is the Larmor radius, m is the electron effective mass, and E_F is the Fermi energy in the 2DEG.

For a cylindrical membrane of radius R:

$$|v_H| \sim \frac{1}{B^2}|\mathrm{grad}\, B_n| = \frac{\sin\varphi}{R B_0 \cos^2\varphi},$$

i.e., in the 2DEG on a cylindrical surface there form sections with different values of the drift velocity of electrons, this velocity in the cycloids located at larger values of φ being greater than that in the vicinity of the region with $B_n = B_0$. Since the charge-carrier mobility is proportional to the drift velocity, one can treat the 2DEG on a cylindrical surface as a set of parallel conductors, each of the conductors featuring its own charge carrier mobility value depending on B_n. A B_n sign change is equivalent to a charge-carrier sign change.

With a turn of the membrane, the distribution of electrons over those conductors undergoes a change. For an estimate, we can represent such a Hall bar with conductors I and II, connected in parallel, both containing charge carries of the same sign whose concentrations are n_1 and n_2, and whose mobilities are respectively μ_1 and μ_2. The Hall voltage for the two types of charge carriers is:

$$U_{xy=} R_{H\mathrm{eff}}\, I\, B_n,$$

where the effective Hall constant $R_{H\mathrm{eff}}$ is given by [22]

$$R_{H\mathrm{eff}} = \frac{\left(\mu_1^2 n_1 + \mu_2^2 n_2\right) + (\mu_1\mu_2 B)^2 (n_1 + n_2)}{e[(\mu_1|n_1| + \mu_2|n_2|)^2 + (\mu_1\mu_2 B)^2 (n_1 + n_2)^2]}.$$

Before calculating μ_1 and μ_2, one has to mention that the gradient drift reduces the electron mobility with respect to the flat 2DEG. This is easy to understand in terms of electron trajectories: in weak gradients, the trajectory is strongly knotted. In strong gradients, the trajectory is much closer to the straight one. So, one can admit that the electron mobility on the cylinder at φ close to 90° is approximately equal to the mobility of the flat 2DEG. Next, we divide the sample into two parts (see inset in Fig. 6) and assume that the electron concentrations in them are $n_1 + n_2 = n$, where n is the concentration in flat 2DEG, and $n_1/n_2 = l_1/l_2$, where l_1 and l_2 are lengths of the segments I and II. The l_1 and l_2 are chosen to be equal ($l_1 = l_2 = l/2$) in case the Hall bar does not cross the $B_n = 0$ line. If one part of the Hall bar is located at $B_n > 0$, and the other one at $B_n < 0$, from geometrical consideration l_1/l_2 can be calculated. We admit that the mobility has the same functional dependence on φ as the drift velocity (2). The mobilities μ_1 and μ_2 are calculated as the mean values in the segments l_1 and l_2,

$$\mu_i = \frac{A}{\varphi - \varphi_i}\int_{l_i} \frac{\sin\varphi}{\cos^2\varphi} d\varphi.$$

The constant A is calculated knowing the maximal mobility ($8 \times 10^4\ \mathrm{cm}^2/\mathrm{V\,s}$) at φ close to 90°.

The results of such calculations are shown on Fig. 6. In the vicinity of $\varphi = 0$ the gradient of B_n is small, and the mobilities μ_1 and μ_2 are nearly identical. For $\varphi = 60°$, the $R_{xy}(B)$ is steeper in weak fields. For $\varphi = 100°$, the $R_{xy}(B)$ slope changes sign. These results are in qualitative agreement with the experimental observations. The same procedure was done for the 75 μm Hall bar [Fig. 6(b)].

Thus, the simple approximation of the charge carriers of two types provides a reasonable explanation to the nonlinearities and their variation observed in the Hall effect in the 2DEG on a cylindrical nanomembrane in classical magnetic fields.

Figure 5 illustrates the case of an extremely large electron mean free path: $l \gg r_c, l \gg W$ (W is the sample width). In the studied structures, we have a situation with $l \approx 1$ μm, which value implies that $l > r_c$ in fields $B_n > 0.125$ T. In weaker fields, scattering processes result in electron transfer between regions with different values of B_n. However, since there is no preferable scattering direction, there remains dependence of drift velocities on φ. For a more adequate description of

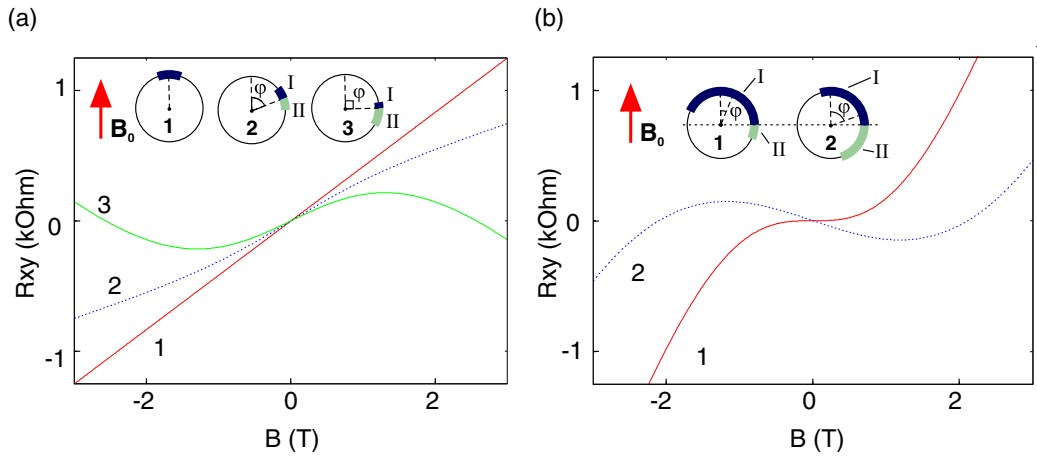

FIG. 6. Calculated dependencies modeling the Hall effect in the (a) 16-μm and (b) 75-μm wide Hall bars.

the effect, both a greater number of the types of charge carries and their redistribution over the sections with different values of B_n have to be taken into account.

A unique feature of our structures with the 2DEG on a cylindrical surface is the possibility to control the shape of electron trajectories and their distribution. On increasing the mobility or on decreasing the shell radius, we expect an emergence of ballistic effects related with the motion of electrons over their trajectories (Fig. 5). Those phenomena may prove interesting from the viewpoint of the local control of electron transport and magnetic focusing [23,24].

In stronger fields (1.5–3.5 T), stepwise Hall dependencies are observed. As R_{xx} does not vanish anywhere in the range of the used fields, the broadened Landau levels overlap and the IQHE regime is not yet reached. Let us discuss the Landau level distribution in 2DEG on the cylindrical surface. The energy gap between Landau levels is given by B_n.

$$E_n = \frac{\hbar e B_n}{m}\left(n+\frac{1}{2}\right) = \frac{\hbar e B_0 \cos\varphi}{m}\left(n+\frac{1}{2}\right).$$

It means that, depending on the angle α between the sector edges, and the angle of rotation φ [Fig. 7(a)], various Landau level distributions are formed [Fig. 7(b)]. In higher fields, when the separation of Landau levels exceeds level broadening, edge states are formed [Fig. 7(c)]. As opposed to the flat 2DEG, 1D conducting channels are additionally formed far from the sample edges. In the quantum Hall regime, the resistances $R_{xx}(B)$ and $R_{xy}(B)$ in cylindrical nanomembranes are to be calculated via summation of the contributions due to all channels with the help of the Landauer-Büttiker formalism [18,19,25]. It is important that the experimental geometry described in the present publication permits the variation of both the distribution of channels and the spacing between the channels in broad ranges right during the experiment (Fig. 7). The latter possibility is unachievable in planar 2DEG, and it opens up additional opportunities for the study of the interaction between the edge channels with codirected or antidirected electron spins and momenta [26].

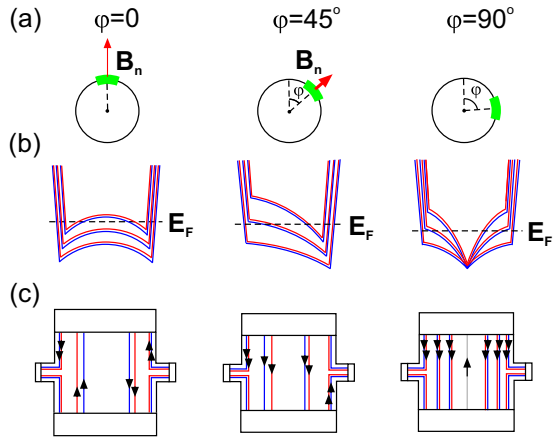

FIG. 7. (a) Schematic illustrating three different orientations of a cylindrical nanomembrane in an external magnetic field. (b) Landau levels in the cylindrical nanomembrane $E_n = \frac{\hbar e B_n}{m}(n+\frac{1}{2}) = \frac{\hbar e B_0 \cos\varphi}{m}(n+\frac{1}{2})$. The red and blue solid lines show the spin-split sublevels. The dashed line is the Fermi level. (c) The point of intersection of the bent Landau levels with the Fermi level gives the spatial position of the 1D channels. The spacing between the channels is defined by the angular position of the membrane with respect to the external magnetic field, and the value of the external magnetic field. The dashed line for $\varphi = 90°$ shows the state in the vicinity of $B_n = 0$, which corresponds to a snakelike trajectory.

IV. CONCLUSION

In the present work we performed a detailed study of the effect due to Lorentz-force gradient on the Hall voltage in 2DEG. To this end, cylindrical nanomembranes with 2DEG were prepared. That was done by directional rolling of strained GaAs-based heterostructures with lithographically defined Hall bars. Experimenting with the width of the bars and with the angle of their rotation in an external magnetic field, we have realized both weak and strong magnetic-field gradients and, also, a sign-alternating magnetic field acting on the 2DEG in the nanomembrane. It was found that an increase in the magnetic-field gradient led to an increase of the Hall constant in weak fields, whereas a change in the field sign, to an inversion of this constant in weak fields. An explanation based on the analysis of the dependence of electron drift velocities on the magnetic field gradient is

proposed. The results of the model calculations fairly well agree with the experiment. The behaviour of the system in quantizing magnetic fields and its potential applications in the areas of basic research and practical applications were discussed.

ACKNOWLEDGMENTS

We thank Dr. G. M. Min'kov and Dr. A. A. Sherstobitov (IMP, UB RAS, Ekaterinburg) for their help with the experimental equipment. The study was supported by the Russian Foundation for Basic Research (Grant No. 17-02-01218).

[1] G. Papp and F. M. Peeters, Appl. Phys. Lett. **78**, 2184 (2001).

[2] L. Dell'Anna and A. De Martino, Phys. Rev. B **80**, 155416 (2009).

[3] J. E. Müller, Phys. Rev. Lett **68**, 385 (1992).

[4] M. Hara, A. Endo, Sh. Katsumoto, and Y. Iye, Phys. Rev. B **69**, 153304 (2004).

[5] A. Nogaret, D. N. Lawton, D. K. Maude, J. C. Portal, and M. Henini, Phys. Rev. B **67**, 165317 (2003).

[6] A. Nogaret, S. Carlton, B. L. Gallagher, P. C. Main, M. Henini, R. Wirtz, R. Newbury, M. A. Howson, and S. P. Beaumont, Phys. Rev. B **55**, R16037(R) (1997).

[7] J. Reijniers and F. M. Peeters, Phys. Rev. B **63**, 165317 (2001).

[8] A. Nogaret, J. Phys.: Condens. Matter **22**, 253201 (2010).

[9] P. D. Ye, D. Weiss, R. R. Gerhardts, M. Seeger, K. von Klitzing, K. Eberl, and H. Nickel, Phys. Rev. Lett. **74**, 3013 (1995).

[10] I. S. Ibrahim, V. A. Schweigert, and F. M. Peeters, Phys. Rev. B **56**, 7508 (1997).

[11] M. L. Leadbeater, C. L. Foden, J. H. Burroughes, M. Pepper, T. M. Burke, L. L. Wang, M. P. Grimshaw, and D. A. Ritchie, Phys. Rev. B **52**, R8629(R) (1995).

[12] A. A. Bykov, G. M. Gusev, J. R. Leite, A. K. Bakarov, N. T. Moshegov, M. Cassé, D. K. Maude, and J. C. Portal, Phys. Rev. B **61**, 5505 (2000).

[13] R. G. Mani, Appl. Phys. Lett. **70**, 2879 (1997).

[14] R. G. Mani, Phys. Rev. B **55**, 15838 (1997).

[15] R. J. F. van Haren, F. A. P. Blom, and J. H. Wolter, Phys. Rev. Lett. **74**, 1198 (1995).

[16] R. Ilan, N. R. Cooper, and A. Stern, Phys. Rev. B **73**, 235333 (2006).

[17] V. Ya. Prinz, V. A. Seleznev, A. K. Gutakovsky, A. V. Chehovskiy, V. V. Preobrazhenskii, M. A. Putyato, and T. A. Gavrilova, Physica E **6**, 828 (2000)

[18] A. B. Vorob'ev, K.-J. Friedland, H. Kostial, R. Hey, U. Jahn, E. Wiebicke, Ju. S. Yukecheva, and V. Ya. Prinz, Phys. Rev. B **75**, 205309 (2007).

[19] Ju. S. Vorobyova, A. B. Vorob'ev, V. Ya. Prinz, A. I. Toropov, and D. K. Maude, Nano Lett. **15**, 1673 (2015).

[20] A. Nogaret, P. Mondal, A. Kumar, S. Ghosh, H. Beere, and D. Ritchie, Phys. Rev. B **96**, 081302(R) (2017).

[21] D. A. Frank-Kamenetskii, *Plasma—The Fourth State of Matter* (Plenum, New York, 1972), p. 81.

[22] M. Grundmann, *The Physics of Semiconductors* (Springer, Berlin, 2006), p. 198.

[23] T. Stegmann, D. E. Wolf, and A. Lorke, New J. Phys. **15**, 113047 (2013).

[24] H. van Houten, C. W. J. Beenakker, J. G. Williamson, M. E. I. Broekaart, P. H. M. van Loosdrecht, B. J. van Wees, J. E. Mooij, C. T. Foxon, and J. J. Harris, Phys. Rev. B **39**, 8556 (1989).

[25] K.-J. Friedland, R. Hey, H. Kostial, A. Riedel, and D. Maude, J. Phys. Conf. Ser. **100**, 042023 (2008).

[26] B. Karmakar, D. Venturelli, L. Chirolli, F. Taddei, V. Giovannetti, R. Fazio, S. Roddaro, G. Biasiol, L. Sorba, V. Pellegrini, and F. Beltram, Phys. Rev. Lett. **107**, 236804 (2011).